



# Facile fabrication of ordered $\text{Si}_{1-x}\text{Ge}_x$ nanostructures via hybrid process of selective epitaxial growth (SEG) and self-assembled nanotemplates

Sang-Joon Park\*, Inchan Hwang, Heung Soon Lee, Sunggi Baik, Hyungjun Kim<sup>1</sup>

Department of Material Science and Engineering, Pohang University of Science and Technology (POSTECH), Pohang 790-784, Republic of Korea

## ARTICLE INFO

### Article history:

Received 22 February 2012  
Received in revised form 17 April 2012  
Accepted 21 April 2012  
Available online 9 May 2012

### Keywords:

Ordered SiGe nanostructures  
Selective epitaxial growth  
Anodic aluminum oxide  
Diblock copolymer

## ABSTRACT

In this study, a facile fabrication method of the ordered  $\text{Si}_{1-x}\text{Ge}_x$  nanodots (NDs) and nanowires (NWs) was successfully developed via hybrid process of selective epitaxial growth (SEG) of  $\text{Si}_{1-x}\text{Ge}_x$  and self-assembled nanotemplates, i.e., anodic aluminum oxide (AAO) and diblock copolymer (DBC) of polystyrene-*b*-polymethylmethacrylate (PS-*b*-PMMA).  $\text{Si}_{1-x}\text{Ge}_x$  films were selectively grown on the Si windows against the oxide area at a growth temperature of 550 °C by repeating the unit cycle consisting of two consecutive steps;  $\text{Si}_{1-x}\text{Ge}_x$  deposition step using  $\text{Si}_2\text{H}_6$  and  $\text{GeH}_4$  and  $\text{Cl}_2$  exposure step for removing the nuclei or deposits formed on the oxide area during the preceding  $\text{Si}_{1-x}\text{Ge}_x$  deposition step. The chemical composition of the  $\text{Si}_{1-x}\text{Ge}_x$  films was readily controlled by adjusting the flow rate of  $\text{GeH}_4$  from 20 sccm to 45 sccm while that of  $\text{Si}_2\text{H}_6$  gas was fixed at 10 sccm, giving rise to the variation of Ge composition in  $\text{Si}_{1-x}\text{Ge}_x$  from 22.2% to 34.0%.

In order to fabricate well-ordered  $\text{Si}_{1-x}\text{Ge}_x$  nanostructures, Si windows with hexagonal arrangement were fabricated using AAO and PS-*b*-PMMA. AAO was prepared through multi-step anodization of the Al films of Al/Si(001) substrate under suitable anodizing conditions. Subsequently, ordered Si windows were fabricated by removing the barrier layer at the bottom of the AAO membrane by reactive ion etching (RIE). In case of PS-*b*-PMMA,  $\text{SiO}_2$  templates with ordered Si windows were fabricated through replication of nano-cylindrical pattern of PS-*b*-PMMA to the 20-nm thick  $\text{SiO}_2$  layers of  $\text{SiO}_2/\text{Si}$ . By utilizing the ordered Si windows obtained from both AAO and PS-*b*-PMMA,  $\text{Si}_{1-x}\text{Ge}_x$  was selectively grown on Si windows against the oxide area, viz., aluminum oxide in AAO and  $\text{SiO}_2$  templates. Hexagonally ordered NDs and freestanding NWs were facily fabricated on the Si substrates after removing the AAO and  $\text{SiO}_2$  templates.

© 2012 Elsevier B.V. All rights reserved.

## 1. Introduction

Various nanostructures such as nanodots (NDs) and nanowires (NWs) have been widely studied due to their unique properties originated from their low dimension [1–6]. They have been expected to play a key role in emerging electronics such as high-sensitivity sensor, energy storage/generation applications, and photonic and optoelectronic devices [7–10]. Among a variety of nanostructure materials,  $\text{Si}_{1-x}\text{Ge}_x$  nanostructures are one of the most representative materials for nanoelectronic applications [10–12]. The most common method for fabrication of  $\text{Si}_{1-x}\text{Ge}_x$  NWs is vapor–liquid–solid (VLS) growth [13–16]. The chemical composition and doping concentration of  $\text{Si}_{1-x}\text{Ge}_x$  such as phos-

\* Corresponding author. Address: Engineering Building #1, Pohang University of Science and Technology (POSTECH), San31, Hyoja-dong, Nam-gu, Pohang, Gyeongbuk 790-784, Republic of Korea. Tel.: +82 54 279 2822; fax: +82 54 279 5090.

E-mail address: [narcciss@postech.ac.kr](mailto:narcciss@postech.ac.kr) (S.-J. Park).

<sup>1</sup> Present address: School of Electrical and Electronic Engineering, Yonsei University, Seoul 120-749, Republic of Korea.

phorus and boron can be facily altered by adjusting the gas flow rates of each Si and Ge source and those of dopant sources during the VLS [16].  $\text{Si}_{1-x}\text{Ge}_x$  NDs are generally fabricated through spontaneous self-organized growth of  $\text{Si}_{1-x}\text{Ge}_x$  on Si substrate, which is originated from their lattice mismatch [17–19]. Precise control of position, size and shape is one of the prerequisite for actual and reliable application of the  $\text{Si}_{1-x}\text{Ge}_x$  nanostructures to practical electronics. Aforementioned fabrication methods of  $\text{Si}_{1-x}\text{Ge}_x$  nanostructures, however, have shown lack of such controllability. Moreover, incorporation of the metal impurity into  $\text{Si}_{1-x}\text{Ge}_x$  is unavoidable in VLS method because of the use of metal catalyst [20], resulting in the degradation of device performance [21].

To resolve these issues of existing fabrication techniques of  $\text{Si}_{1-x}\text{Ge}_x$  nanostructures, we employed the selective epitaxial growth (SEG). SEG has recently drawn huge attention as one of the promising catalyst-free fabrication methods of nanostructured semiconductors including  $\text{Si}_{1-x}\text{Ge}_x$  [22], Ge [23], and GaN [24]. In an attempt to deliberately control the position and composition of  $\text{Si}_{1-x}\text{Ge}_x$  nanostructures, i.e., NWs and NDs, we employed the hybrid process of  $\text{Si}_{1-x}\text{Ge}_x$  SEG and self-assembled nanotemplates.

In this study, we adopted two different kinds of nanotemplates; one is anodic aluminum oxide (AAO) and the other is diblock copolymer (DBC). Both of nanotemplates exhibit the regularly arranged nanopatterns [25–27]. They have been widely used for the purpose of fabricating the nanostructured materials [24,28–31]. For the case of AAO, vertically penetrated and hexagonally arranged cylindrical nanoholes are readily formed by anodizing aluminum under the proper anodizing conditions; electrolytes, temperature, applied voltage or current [25,27]. The hole dimension including the diameter and length can be easily controlled by simply varying the anodizing voltages, times, and additional pore-widening. On the other hand, for the case of DBC, various nanopatterns such as sphere, lamella, and cylinder can be fabricated through the microphase separation of DBC, in which the shape of the nanopattern can be altered by simply changing the molecular weight of each polymer block [26,29,30]. Among a diversity of the nanopatterns which can be obtained from DBC, cylindrical nanohole pattern is advantageous in fabricating the nanostructures which directly contact on the substrates by virtue of direct formation of nanoholes normal to the surface of substrates.

In SEG,  $\text{Si}_{1-x}\text{Ge}_x$  is preferentially well grown on the Si surfaces, whereas it is rarely deposited on the oxide or nitride ones [32–34]. Enabled by this selective growth characteristic of SEG, we developed the facile fabrication method for ordered and composition-controlled  $\text{Si}_{1-x}\text{Ge}_x$  nanostructures, i.e., hybrid process of  $\text{Si}_{1-x}\text{Ge}_x$  SEG and self-assembled nanotemplates.  $\text{Si}_{1-x}\text{Ge}_x$  SEG with good selectivity between Si windows and oxide layer was established by repeating the unit cycle of SEG composed of two consecutive steps; one is  $\text{Si}_{1-x}\text{Ge}_x$  growth step by ultra-high vacuum chemical deposition (UHV-CVD) using pure disilane ( $\text{Si}_2\text{H}_6$ ) and germane ( $\text{GeH}_4$ ) gases and the other is etching step of small  $\text{Si}_{1-x}\text{Ge}_x$  nuclei or deposits, which might have been formed on oxide layer during the preceding  $\text{Si}_{1-x}\text{Ge}_x$  growth step, by introducing pure chloride ( $\text{Cl}_2$ ) gas to reaction chamber. Two different types of nano-sized Si windows were fabricated by employing the nanotemplates; AAO and DBC nanotemplates polystyrene-block-polymethylmethacrylate (PS-*b*-PMMA). One is Si windows surrounded with aluminum oxide of AAO template, which was prepared by anodizing Al layer directly deposited on Si substrate and subsequently removing the barrier layer of the holes of AAO. The other ones were fabricated using the hexagonal nanohole arrays of PS templates obtained from PS-*b*-PMMA. Ordered Si windows were prepared via transfer of nanohole pattern of PS templates to  $\text{SiO}_2$  layer by  $\text{CF}_4$  reactive ion etching (RIE) by utilizing PS as an etching mask. Hexagonally well ordered  $\text{Si}_{1-x}\text{Ge}_x$  NDs were fabricated on Si(001) substrate through  $\text{Si}_{1-x}\text{Ge}_x$  SEG on the resulting Si windows and subsequent removal of the oxide layers of aluminum oxide and  $\text{SiO}_2$ . Moreover, vertically aligned free standing  $\text{Si}_{1-x}\text{Ge}_x$  NWs with uniform diameter were readily fabricated on Si(001) substrate using the Si windows with thick AAO templates by increasing the number of  $\text{Si}_{1-x}\text{Ge}_x$  SEG cycle. The lateral size of the resulting  $\text{Si}_{1-x}\text{Ge}_x$  NDs and NWs were found to exhibit the good agreement with the hole size of AAO and PS-*b*-PMMA.

## 2. Experimental details

### 2.1. Fabrication of ordered Si windows

As shown in the schematic diagrams of Fig. 1, hexagonally ordered Si windows with sub-100 nm in lateral dimension were fabricated via two different processes using AAO (Fig. 1a) and PS-*b*-PMMA (Fig. 1b).

#### 2.1.1. Fabrication of Si windows using AAO

The first type of Si window was prepared using AAO. The AAO was prepared by anodizing the 1.4- $\mu\text{m}$  thick Al film, which had been thermally evaporated on the Si(001) substrate. Multi-step anodization was employed in order to improve hole

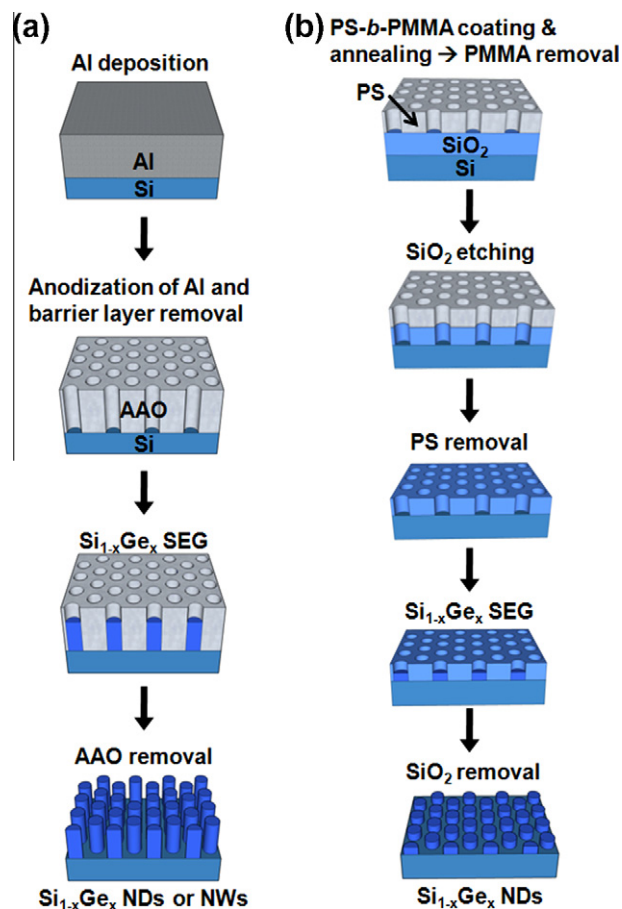
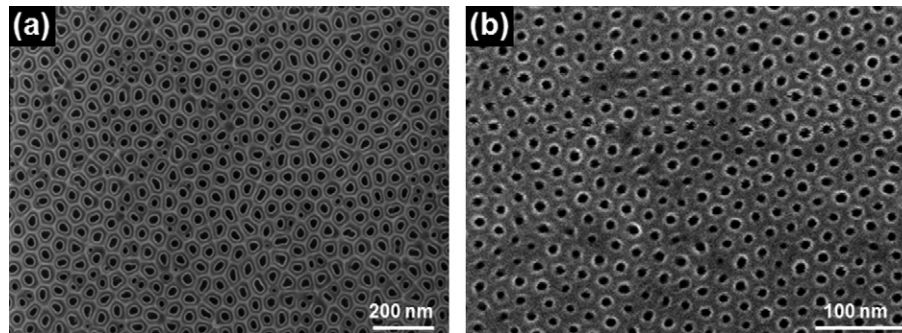


Fig. 1. Schematic diagrams for two different ways of  $\text{Si}_{1-x}\text{Ge}_x$  nanostructures fabrication using (a) AAO templates and (b) PS-*b*-PMMA.

ordering of AAO [35]. A carbon counter electrode and Si substrate with Al film were dipped into the electrolyte of 0.3 M oxalic acid. Anodization was performed under the applied voltage of 40 V at 15 °C. The AAO membrane formed during the 1st anodization step was removed by dipping the sample into the mixture solution of chromic and phosphoric acid, which was maintained at 65 °C. After repeating these two steps several times alternately and carrying out the final anodization step, the hexagonally ordered hole arrays were obtained at last. The thickness of AAO membrane could be controlled by adjusting the duration of the final anodization step in consideration of the pursued AAO thickness. Fig. 2a is the SEM image for the resulting AAO template, prepared by anodizing the Al film on Si. The hole diameter was enlarged to 70 nm by dipping AAO template into the 0.1 M phosphoric acid solution which was maintained at 30 °C. In order to fabricate the exposed Si window at each of nanoholes, the barrier layer of AAO was etched away by reactive ion etching (RIE) using the mixture gas of 20-sccm  $\text{BCl}_3$  and 10-sccm Ar under the same power of 150 W for source and bias of plasma. The etching duration was altered depending on the AAO thickness; the longer the AAO thickness was, the longer etching duration to remove the barrier layer was.

#### 2.1.2. Fabrication of Si windows using PS-*b*-PMMA

The Si windows were also fabricated by using DBC of PS-*b*-PMMA in order to fabricate the Si windows with smaller size of 20-nm diameter in comparison those prepared by utilizing the AAO. The Si windows with the nanohole-patterned  $\text{SiO}_2$  template was obtained through pattern transfer of hexagonally ordered nanoholes of PS-*b*-PMMA to 20-nm thick  $\text{SiO}_2$  layer on Si(001) substrate. Self-assembled monolayer (SAM) of 3-(*p*-methoxy-phenyl)propyltrichloro-silane [MPTS,  $\text{CH}_3\text{OPh}(\text{CH}_2)_3\text{SiCl}_3$ ] was coated on  $\text{SiO}_2/\text{Si}$  substrate prior to PS-*b*-PMMA coating, leading to the hydrophobically neutral surface of the substrate. During the vacuum annealing of PS-*b*-PMMA-coated Si substrate at 180 °C for 24 h, microphase separation of PMMA and PS took place, resulting in PMMA nanocylinder and PS matrix. The ordering of PMMA cylinders was facilitated by virtue of the hydrophobically neutral substrate surface. Finally, vertically aligned cylindrical nanoholes were formed on the  $\text{SiO}_2/\text{Si}$  substrates as a consequence of removal of the PMMA cylinders by performing ultra-violet (UV) exposure to the sample for 90 min, giving rise to degradation of the PMMA, and subsequent dipping of sample into the glacial acetic acid for 1 min. Fig. 2b shows the resulting 20-nm diameter hole array fabricated by utilizing



**Fig. 2.** Top-view SEM images: (a) AAO fabricated through multi-step anodization of the Al films evaporated on the Si substrate, (b) cylindrical nanoholes formed on the Si with native oxide using PS-*b*-PMMA.

PS-*b*-PMMA. By using this nanohole pattern, SiO<sub>2</sub> template with ordered nanoholes was fabricated through the nanocylindrical pattern transfer of PS-*b*-PMMA to 20-nm thick SiO<sub>2</sub> layer of SiO<sub>2</sub>/Si by CF<sub>4</sub> RIE. In the end, ordered Si windows of diameter of 20 nm were obtained. More details for these were reported by our previous study [36].

## 2.2. Si<sub>1-x</sub>Ge<sub>x</sub> nanostructure fabrication by the Si<sub>1-x</sub>Ge<sub>x</sub> SEG

Si<sub>1-x</sub>Ge<sub>x</sub> was grown by UHV-CVD at a growth temperature of 550 °C. SEG of Si<sub>1-x</sub>Ge<sub>x</sub> on the Si windows was achieved by repeating the unit cycle of SEG, which was composed of two separate steps, namely, the Si<sub>1-x</sub>Ge<sub>x</sub> deposition step and the Cl<sub>2</sub> exposure step to etch away the Si<sub>1-x</sub>Ge<sub>x</sub> nuclei or deposits which could be formed on oxide layer during the preceding Si<sub>1-x</sub>Ge<sub>x</sub> deposition step. During the Si<sub>1-x</sub>Ge<sub>x</sub> deposition step of 20 s, pure GeH<sub>4</sub> and Si<sub>2</sub>H<sub>6</sub> gases were introduced to the reaction chamber at a flow rate of 20 and 10 sccm, respectively. On the other hand, during the Si<sub>1-x</sub>Ge<sub>x</sub> etching step, samples were exposed to Cl<sub>2</sub> gas of flow rate of 1 sccm in an attempt to remove the Si<sub>1-x</sub>Ge<sub>x</sub> nuclei or deposits which could be formed on the oxide area, viz., aluminum oxide of AAO templates or SiO<sub>2</sub> templates obtained using PS-*b*-PMMA in this study. The Si<sub>1-x</sub>Ge<sub>x</sub> thicknesses were controlled by altering the number of cycles of the Si<sub>1-x</sub>Ge<sub>x</sub> SEG.

Si<sub>1-x</sub>Ge<sub>x</sub> nanostructures including NDs and NWs were fabricated through Si<sub>1-x</sub>Ge<sub>x</sub> SEG on Si windows. The numbers of cycles of Si<sub>1-x</sub>Ge<sub>x</sub> SEG were adjusted depending on the pursuing dimensions of Si<sub>1-x</sub>Ge<sub>x</sub> nanostructures, i.e., the height of NDs or the length of NWs. The morphology and the shapes of Si<sub>1-x</sub>Ge<sub>x</sub> nanostructures were observed using atomic force microscopy (AFM), scanning electron microscopy (SEM), high-resolution transmission electron microscopy (HRTEM), and scanning tunneling electron microscopy (STEM). The quantitative chemical composition as well as epitaxial growth of Si<sub>1-x</sub>Ge<sub>x</sub> was analyzed by high-resolution X-ray diffraction (HR-XRD). The qualitative composition analysis on Si<sub>1-x</sub>Ge<sub>x</sub> NWs was performed by the energy-dispersive spectroscopy (EDS) mapping. The crystal-line structure of the Si<sub>1-x</sub>Ge<sub>x</sub> NDs was investigated by HR-XRD at Pohang Accelerator Laboratory (PAL).

## 3. Results and discussion

### 3.1. Si<sub>1-x</sub>Ge<sub>x</sub> film deposition on Si(001) substrates & control of its chemical composition

The chemical composition of the Si<sub>1-x</sub>Ge<sub>x</sub> films was modulated by adjusting the flow rate of the precursor gas of Ge (i.e., GeH<sub>4</sub>) while that of Si precursor gas (i.e., Si<sub>2</sub>H<sub>6</sub>) was fixed at 10 sccm. Table 1 presents the effect of the flow rate of each precursor gas of Si<sub>2</sub>H<sub>6</sub> and GeH<sub>4</sub>, and the resulting chemical composition of Si<sub>1-x</sub>Ge<sub>x</sub> prepared at different conditions of precursor gases. As described in Table 1, the chemical composition of Ge in the present Si<sub>1-x</sub>Ge<sub>x</sub> films was adjusted from 22.2% to 34.0% depending growth condi-

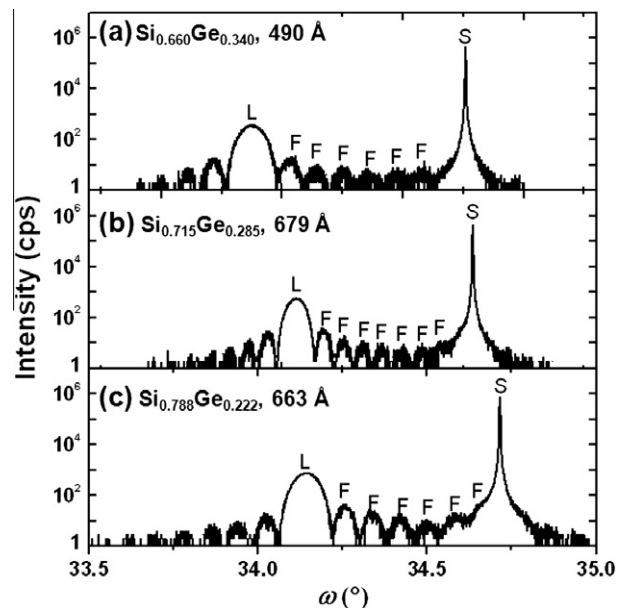


**Fig. 3.** HR-XRD  $\omega - 2\theta$  scan spectra of Si<sub>1-x</sub>Ge<sub>x</sub> films grown with different flow rates of GeH<sub>4</sub> and a fixed flow rate of 10 sccm of Si<sub>2</sub>H<sub>6</sub>. The each of spectra were measured normal to Si(004) plane: (a) 45-sccm GeH<sub>4</sub>, Si<sub>0.660</sub>Ge<sub>0.340</sub>; (b) 31-sccm GeH<sub>4</sub>, Si<sub>0.715</sub>Ge<sub>0.285</sub>; (c) 20-sccm GeH<sub>4</sub>, Si<sub>0.788</sub>Ge<sub>0.222</sub>. (S: Diffraction peak from Si(004), L: diffraction peak from Si<sub>1-x</sub>Ge<sub>x</sub> layer, and F: Fringe peaks originated from interference between Si and Si<sub>1-x</sub>Ge<sub>x</sub>)

tions, viz., the flow rates of Si<sub>2</sub>H<sub>6</sub> and GeH<sub>4</sub>. The chemical compositions of each Si and Ge in the resulting Si<sub>1-x</sub>Ge<sub>x</sub> films were determined from the difference of diffraction angle between Si(004) and Si<sub>1-x</sub>Ge<sub>x</sub>(004) in  $\omega - 2\theta$  scan spectra, which is originated from the larger lattice constant of Si<sub>1-x</sub>Ge<sub>x</sub> than that of Si. Fig. 3 shows the  $\omega - 2\theta$  scan spectra of the resulting Si<sub>1-x</sub>Ge<sub>x</sub> films. As manifested by Fig. 3, the distinct diffraction peaks of Si<sub>1-x</sub>Ge<sub>x</sub> (004) as well as fringe peaks observed in  $\omega - 2\theta$  spectra supply a evidence on the high quality Si<sub>1-x</sub>Ge<sub>x</sub> film deposition by our deposition process. More details for chemical composition control and growth behaviors of our Si<sub>1-x</sub>Ge<sub>x</sub> films will be reported elsewhere.

**Table 1**

Chemical composition of Si<sub>1-x</sub>Ge<sub>x</sub> films grown under different gas flow rates of Si<sub>2</sub>H<sub>6</sub> and GeH<sub>4</sub>.

		Condition I	Condition II	Condition III
Precursor gas flow rate (sccm)	Si <sub>2</sub> H <sub>6</sub>	10	10	10
	GeH <sub>4</sub>	20	31	45
Ge composition (%)		22.2	28.5	34.0
Chemical formula		Si <sub>0.788</sub> Ge <sub>0.222</sub>	Si <sub>0.715</sub> Ge <sub>0.285</sub>	Si <sub>0.660</sub> Ge <sub>0.340</sub>

### 3.2. Fabrication of $\text{Si}_{1-x}\text{Ge}_x$ NDs and NWs using AAO

Prior to applying  $\text{Si}_{1-x}\text{Ge}_x$  SEG to the nano-sized Si windows, the reliable selective growth of  $\text{Si}_{1-x}\text{Ge}_x$  was checked out using the square-shaped Si windows with various sizes, which were formed in 200-nm thick  $\text{SiO}_2$  layers on Si substrates. The  $\text{Si}_{1-x}\text{Ge}_x$  SEG was achieved by repeating the unit cycle of two sequential steps of  $\text{Si}_{1-x}\text{Ge}_x$  film deposition and  $\text{Cl}_2$  exposure step to eliminate the  $\text{Si}_{1-x}\text{Ge}_x$  nuclei or deposits which could be formed on oxide layer. During the former step of 20 s,  $\text{Si}_2\text{H}_6$  and  $\text{GeH}_4$  were introduced to reaction chamber at flow rates of 20 and 10 sccm, respectively. On the other hand, during the  $\text{Cl}_2$  exposure step of 10 s, 1 sccm of  $\text{Cl}_2$  gas was delivered to the reaction chamber.

From  $\text{Si}_{1-x}\text{Ge}_x$  SEG on the Si windows of which minimum size is  $500 \times 500 \text{ nm}^2$ , it turned out that  $\text{Si}_{1-x}\text{Ge}_x$  films were selectively grown on the Si windows against on the  $\text{SiO}_2$  area. In other word,  $\text{Si}_{1-x}\text{Ge}_x$  SEG by our approach was successfully developed. The good selectivity of our  $\text{Si}_{1-x}\text{Ge}_x$  SEG was also confirmed when it was carried out on the substrate of an array of via holes in  $\text{SiO}_2$ . The aspect ratio of a via hole was 1:5; the diameter of the top and the bottom of a via hole was 95 and 82 nm, respectively and the depth of them was 470 nm. The bottom of as-received via holes was covered by thin  $\text{SiN}_x$  etch-stop layer on Si substrates, leading to no  $\text{Si}_{1-x}\text{Ge}_x$  growth on the nitride layer at the bottom of via holes even after 450 cycles of  $\text{Si}_{1-x}\text{Ge}_x$  SEG. In order to obtain the exposed Si surface at the bottom of each via hole, prior to carrying out  $\text{Si}_{1-x}\text{Ge}_x$  SEG,  $\text{SiN}_x$  layer was selectively etched by dipping samples into 85% phosphoric acid heated at 160 °C for 5 min. Subse-

quent 450 cycles of  $\text{Si}_{1-x}\text{Ge}_x$  SEG exhibited the good selective growth of  $\text{Si}_{1-x}\text{Ge}_x$  on the Si windows at the bottom of each of via holes as shown in Fig. 4. The faceting of the  $\text{Si}_{1-x}\text{Ge}_x$  observed in the SEM image is commonly observed in  $\text{Si}_{1-x}\text{Ge}_x$  SEG on the finite areas [37]. On the basis of the results of two preliminary tests, we can conclude that our  $\text{Si}_{1-x}\text{Ge}_x$  SEG has a great feasibility of selective growth on the Si windows of small lateral size down to 100 nm and high aspect ratio, and fabrication of  $\text{Si}_{1-x}\text{Ge}_x$  nanostructures using nano-sized Si windows.

Fig. 5 shows the  $\text{Si}_{1-x}\text{Ge}_x$  nanodots (NDs) fabricated on Si substrate through  $\text{Si}_{1-x}\text{Ge}_x$  SEG on the 70-nm-diameter Si windows, obtained from 150-nm thick AAO template. After 20 cycles of SEG,  $\text{Si}_{1-x}\text{Ge}_x$  was selectively grown on the Si windows at the bottom of each hole of AAO (Fig. 5a), and ordered  $\text{Si}_{1-x}\text{Ge}_x$  NDs were successfully obtained after removing the AAO using the mixture solution of chromic and phosphoric acid (Fig. 5b) at a temperature of 60 °C. The average diameter and inter-dot distance was 70 and 100 nm, respectively.  $\text{Si}_{1-x}\text{Ge}_x$  ND arrays showed the good replication of the hole size and inter-hole distance as well as hexagonal ordering of AAO. During the anodization of Al film deposited on the Si substrate, silicon oxide could be formed beneath the barrier layer of AAO [38]. Complying with this, it can be thought that silicon oxide was remained even after removing the barrier layer of the AAO by RIE, resulting in non-uniform formation of  $\text{Si}_{1-x}\text{Ge}_x$  NDs and different height of each  $\text{Si}_{1-x}\text{Ge}_x$  dot. In other words, remained silicon oxide hindered or retarded the nucleation of the  $\text{Si}_{1-x}\text{Ge}_x$  on the Si windows of the barrier-layer-etched holes of AAO, causing no growth of  $\text{Si}_{1-x}\text{Ge}_x$  or different height of each  $\text{Si}_{1-x}\text{Ge}_x$  NDs.

HRTEM and HR-STEM images of Fig. 6 show the epitaxial growth of  $\text{Si}_{1-x}\text{Ge}_x$  NDs on the Si windows. It is noteworthy that  $\text{Si}_{1-x}\text{Ge}_x$  was epitaxially grown on the Si windows. Epitaxial growth of  $\text{Si}_{1-x}\text{Ge}_x$  also confirmed in the result of HR-XRD. Fig. 7 is the curve for  $\omega - 2\theta$  scan normal to  $\text{Si}(004)$  plane for  $\text{Si}_{1-x}\text{Ge}_x$  ND arrays, presenting the epitaxial growth of SiGe dots, which is in consistent with the STEM results. The curve of  $\omega - 2\theta$  scan is the typical one for  $\text{Si}_{1-x}\text{Ge}_x$  film epitaxially grown on the  $\text{Si}(001)$  substrate [39]. Discernible diffraction peak originated from  $\text{Si}_{1-x}\text{Ge}_x$  was appeared at the  $2\theta$  of  $68.4^\circ$  although the different peak of  $\text{Si}_{1-x}\text{Ge}_x$  was relatively broad. The smaller diffraction angle of  $\text{Si}_{1-x}\text{Ge}_x$  (004) than that of Si (004) is due to larger lattice constant of the resulting  $\text{Si}_{1-x}\text{Ge}_x$  than that of Si.

$\text{Si}_{1-x}\text{Ge}_x$  NWs were fabricated using 700-nm thick AAO template, which is thicker than that used in  $\text{Si}_{1-x}\text{Ge}_x$  NDs fabrication, as shown in the SEM images of Fig. 8.  $\text{Si}_{1-x}\text{Ge}_x$  SEG of 450 cycles was carried out on the Si windows and  $\text{Si}_{1-x}\text{Ge}_x$  NWs were obtained after subsequent removal of AAO template. Non-uniform length of each NW may be ascribed to the residual oxide layer on the Si windows, which is the same reason as non-uniform

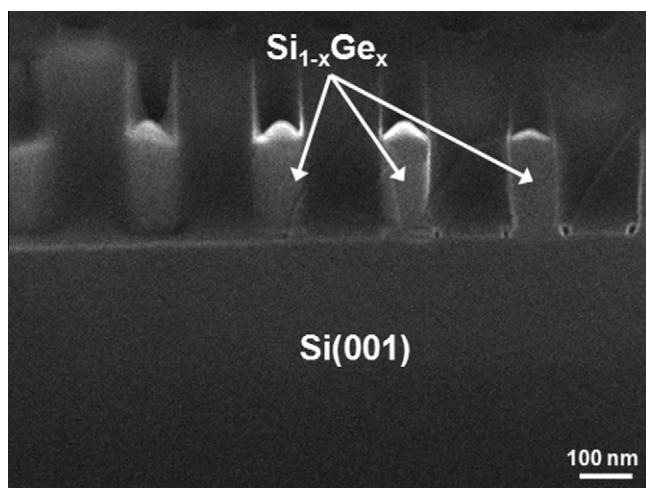


Fig. 4.  $\text{Si}_{1-x}\text{Ge}_x$  selectively grown on via holes during the 450 cycles of  $\text{Si}_{1-x}\text{Ge}_x$  SEG at a growth temperature of 550 °C.

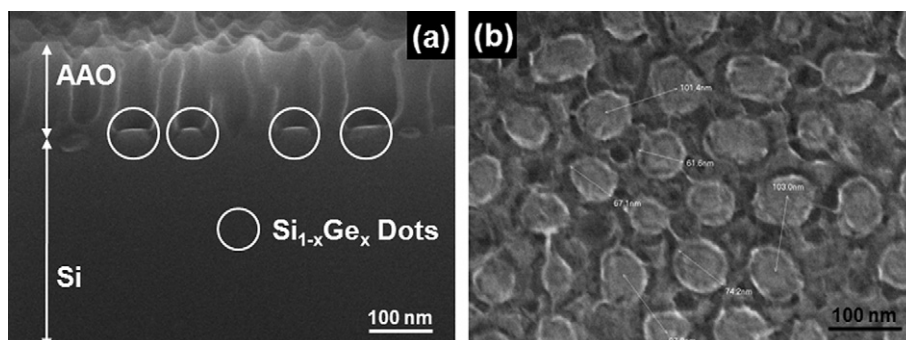


Fig. 5. SEM images of  $\text{Si}_{1-x}\text{Ge}_x$  NDs fabricated on the Si windows, which were fabricated using 200-nm thick AAO template, through 20 cycles of  $\text{Si}_{1-x}\text{Ge}_x$  SEG: (a) cross sectional image before removing AAO and (b) top-view image after removing AAO.

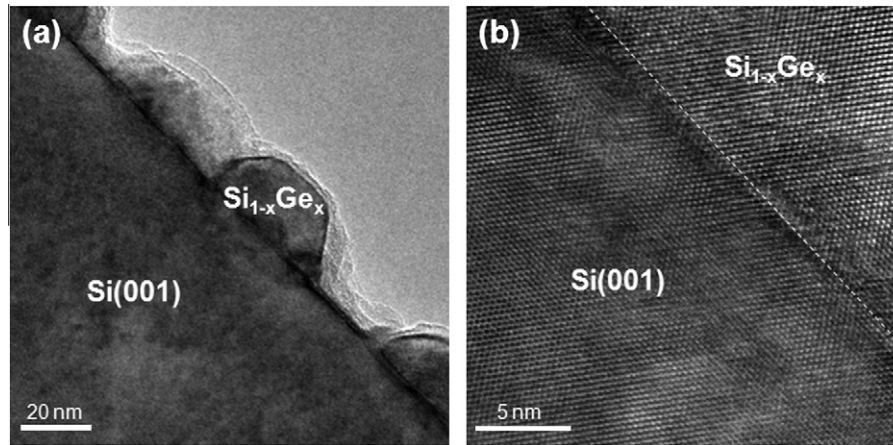


Fig. 6. (a) Cross-sectional view HRTEM images of  $\text{Si}_{1-x}\text{Ge}_x$  NDs and (b) HR-STEM image for the interface between  $\text{Si}_{1-x}\text{Ge}_x$  layer and  $\text{Si}(001)$  substrate.

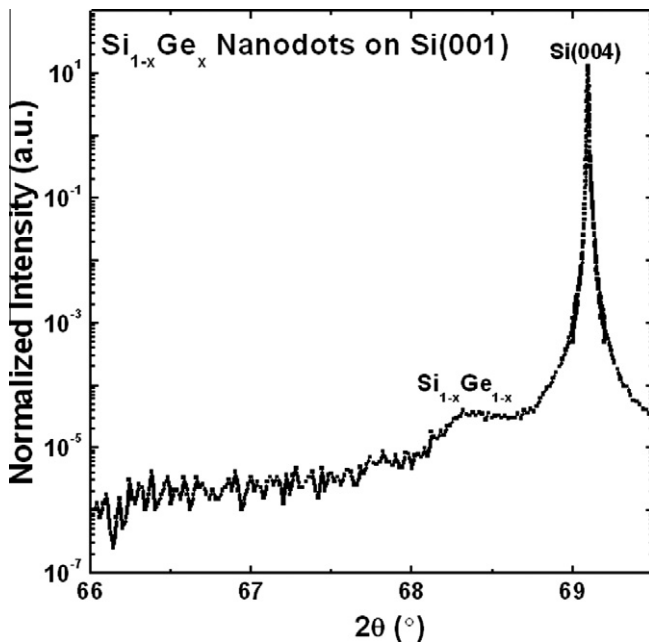


Fig. 7. HR-XRD curve of  $\omega - 2\theta$  scan normal to  $\text{Si}(004)$  plane for  $\text{Si}_{1-x}\text{Ge}_x$  NDs.

formation of  $\text{Si}_{1-x}\text{Ge}_x$  NDs on the Si windows. Clearer elimination process of residual oxide can improve the uniformity of fabrication of  $\text{Si}_{1-x}\text{Ge}_x$  NDs and NWs by SEG.

Energy-dispersive spectroscopy (EDS) mapping result of Fig. 9 revealed that  $\text{Si}_{1-x}\text{Ge}_x$  was selectively grown on the Si windows

formed in the hole of AAO template. It should be noted that  $\text{Si}_{1-x}\text{Ge}_x$  was grown only on the Si but not on AAO, i.e., alumina, presenting  $\text{Si}_{1-x}\text{Ge}_x$  NWs fabrication without using metal catalysts. In addition, Al contamination, probably come from AAO, was also not detected (data not shown). It is obvious that pure  $\text{Si}_{1-x}\text{Ge}_x$  was selectively well grown on the Si windows against aluminum oxide of AAO even after  $\text{Si}_{1-x}\text{Ge}_x$  SEG of 450 cycles.

The hybrid process of  $\text{Si}_{1-x}\text{Ge}_x$  SEG and AAO nanotemplates will be promising method for facile  $\text{Si}_{1-x}\text{Ge}_x$  nanostructures fabrication because  $\text{Si}_{1-x}\text{Ge}_x$  nanostructures, viz., NDs and NWs, can be fabricated without metal catalysts and incorporation of metal impurities via our method. This also can be applied to fabrication of Si and Ge nanostructures. As mentioned earlier, dimension of AAO, namely, hole dimension, inter-hole distance, and depth of hole, is readily modulated by simply adjusting the anodization conditions and additional pore-widening. Based on this, dimensions of  $\text{Si}_{1-x}\text{Ge}_x$  NDs and NWs in our approach can be facilely controlled by employing AAO templates with the variety of hole dimensions. Additionally, the axial length scale of the NDs and NWs can be varied depending on the number of cycles of  $\text{Si}_{1-x}\text{Ge}_x$  SEG.

### 3.3. Fabrication of $\text{Si}_{1-x}\text{Ge}_x$ NDs using PS-*b*-PMMA

To gain more insight into applicability of our approach for fabrication of  $\text{Si}_{1-x}\text{Ge}_x$  nanostructure with smaller size,  $\text{Si}_{1-x}\text{Ge}_x$  SEG was applied to the 20-nm thick  $\text{SiO}_2$  template with ordered circular-shaped Si windows of which diameter was 20 nm. Twenty-cycles  $\text{Si}_{1-x}\text{Ge}_x$  SEG was performed on  $\text{SiO}_2$  template. Good selective growth of  $\text{Si}_{1-x}\text{Ge}_x$  was observed as shown in Fig. 10. Fig. 10a and b are the SEM images of  $\text{SiO}_2$  template after 20-cycles  $\text{Si}_{1-x}\text{Ge}_x$

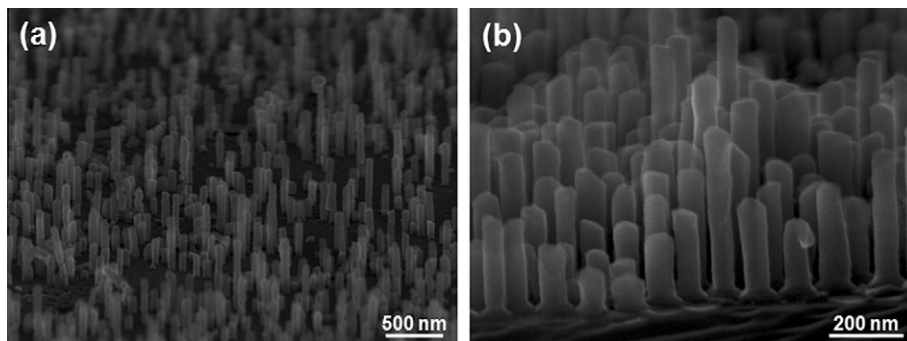


Fig. 8. SEM images for  $\text{Si}_{1-x}\text{Ge}_x$  NWs fabricated on the Si windows through 450 cycles of  $\text{Si}_{1-x}\text{Ge}_x$  SEG. Si windows were fabricated using 450-nm thick AAO.

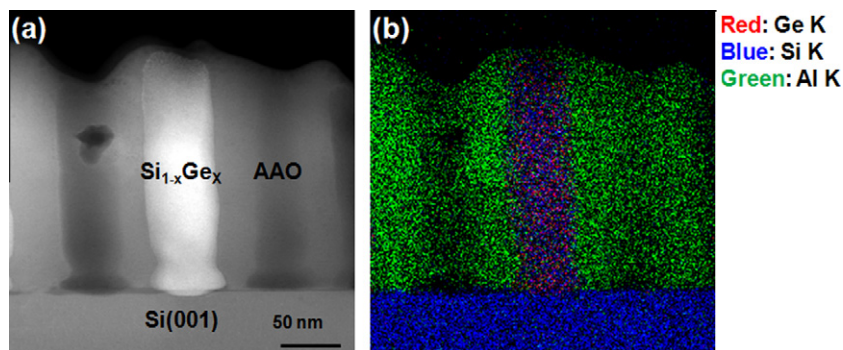


Fig. 9. (a) Bright field TEM image and (b) EDS mapping result for  $\text{Si}_{1-x}\text{Ge}_x$  NW fabricated in a hole of AAO.

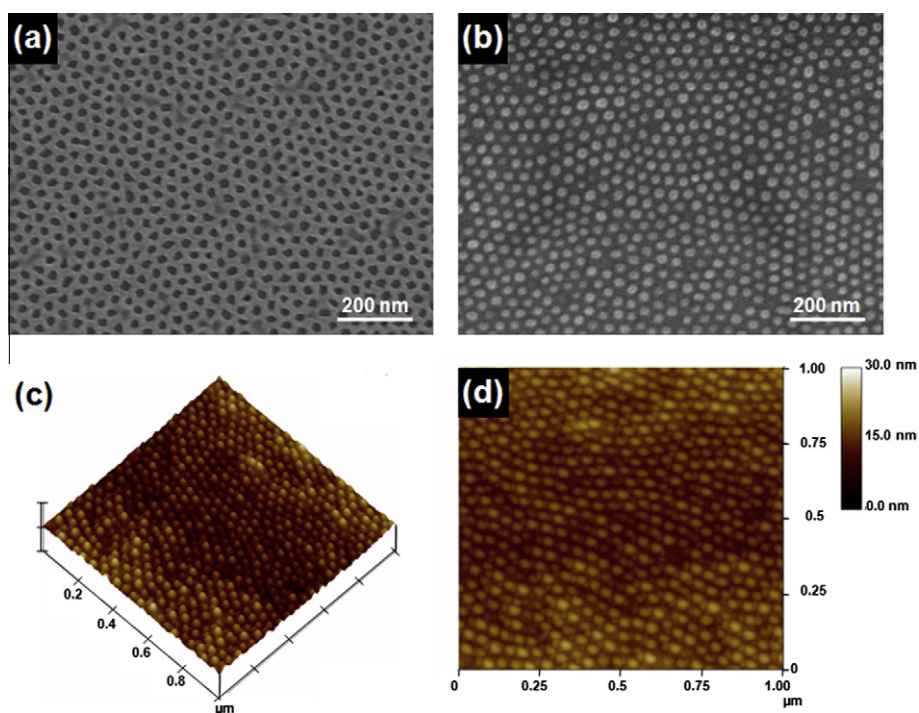


Fig. 10. SEM top-view images of  $\text{Si}_{1-x}\text{Ge}_x$  NDs (a) before and (b) after removing  $\text{SiO}_2$  template.  $\text{Si}_{1-x}\text{Ge}_x$  were selectively grown during the 20 cycles of SEG on the Si windows with 20-nm thick  $\text{SiO}_2$  template, fabricated using PS-*b*-PMMA. (c) and (d) AFM images of  $\text{Si}_{1-x}\text{Ge}_x$  NDs of Fig. 10(b): (c) oblique view and (d) plan-view image (scan size:  $1\ \mu\text{m} \times 1\ \mu\text{m}$ , Z-scale: 50 nm).

SEG and ordered  $\text{Si}_{1-x}\text{Ge}_x$  NDs obtained after taking away  $\text{SiO}_2$  template, respectively. As shown in Fig. 10a, hexagonally arranged nanohole pattern was well replicated to the  $\text{SiO}_2$  layers through transfer of hexagonal nanohole pattern of PS-*b*-PMMA.  $\text{Si}_{1-x}\text{Ge}_x$  was selectively grown on the Si windows against  $\text{SiO}_2$  area and finally  $\text{Si}_{1-x}\text{Ge}_x$  NDs were fabricated on the Si substrate after removing the  $\text{SiO}_2$  layer. Hexagonal arrangement of the resulting  $\text{Si}_{1-x}\text{Ge}_x$  NDs was observed using AFM measurements as shown in Fig. 10c and d. As confirmed from the SEM and AFM measurements, ordered  $\text{Si}_{1-x}\text{Ge}_x$  NDs were successfully fabricated on the Si substrates via  $\text{Si}_{1-x}\text{Ge}_x$  SEG on an array of 20-nm-diameter Si windows. This result presents that the small size of  $\text{Si}_{1-x}\text{Ge}_x$  nanostructures down to size of 20 nm or even smaller scale can be fabricated by our hybrid process which employ the  $\text{Si}_{1-x}\text{Ge}_x$  SEG and DBCs.

#### 4. Conclusions

In this study, a facile fabrication method for the ordered  $\text{Si}_{1-x}\text{Ge}_x$  nanostructures such as nanodots (NDs) and nanowires

(NWs) was successfully developed via hybrid process of selective epitaxial growth (SEG) of  $\text{Si}_{1-x}\text{Ge}_x$  and self-assembled nanotemplates, i.e., anodic aluminum oxide (AAO) and diblock copolymer (DBC) of polystyrene-*b*-polymethylmethacrylate (PS-*b*-PMMA).  $\text{Si}_{1-x}\text{Ge}_x$  films were selectively grown on the Si windows against the oxide area at a growth temperature of 550 °C by repeating the unit cycles consisting of two consecutive steps;  $\text{Si}_{1-x}\text{Ge}_x$  deposition step and  $\text{Cl}_2$  exposure step. During the former step, in order for the  $\text{Si}_{1-x}\text{Ge}_x$  to be grown,  $\text{Si}_2\text{H}_6$  and  $\text{GeH}_4$  were injected to the reaction chamber as a Si and Ge gas source, respectively. Meanwhile, during the latter step,  $\text{Cl}_2$  was introduced to the reaction chamber to achieve the SEG on the Si windows, resulting from etching of the nuclei or deposits formed on oxide area during the preceding  $\text{Si}_{1-x}\text{Ge}_x$  deposition step. The chemical composition of the  $\text{Si}_{1-x}\text{Ge}_x$  films was controlled by adjusting the flow rate of  $\text{GeH}_4$  from 20 sccm to 45 sccm while that of Si gas source was fixed at 10 sccm, giving rise to the variation of Ge composition in  $\text{Si}_{1-x}\text{Ge}_x$  from 22.2% to 34.0%.

The position, direction, and density as well as dimension of nanostructures should be deliberately controlled for their applica-

tion to practical applications. To this end, in this study, hexagonally ordered Si windows were utilized in order to fabricate the  $\text{Si}_{1-x}\text{Ge}_x$  NDs and NWs. Hexagonal arrangement of the Si windows was replicated from the cylindrical nanohole arrays of self-assembled nanotemplates, viz., AAO and PS-*b*-PMMA. AAO was prepared through multi-step anodization of the Al films deposited on Si(001) substrate, under suitable anodizing conditions. Ordered nanohole arrays were also obtained from the PS-*b*-PMMA by adjusting the molecular weight of each polymer block of PS and PMMA. In case of AAO, Si windows were easily fabricated by removing the barrier layer at the bottom of each nanohole of AAO using reactive ion etching (RIE). In case of PS-*b*-PMMA,  $\text{SiO}_2$  templates with ordered Si windows were fabricated through replication of nanocylindrical pattern of PS-*b*-PMMA to the 20-nm thick  $\text{SiO}_2$  layers of  $\text{SiO}_2/\text{Si}$ . By utilizing the ordered Si windows obtained from both AAO and PS-*b*-PMMA,  $\text{Si}_{1-x}\text{Ge}_x$  was selectively grown on the Si windows against the oxide area, i.e., aluminum oxide in AAO and  $\text{SiO}_2$  templates.  $\text{Si}_{1-x}\text{Ge}_x$  SEG was successfully fulfilled on the Si windows, and hexagonally ordered  $\text{Si}_{1-x}\text{Ge}_x$  ND and freestanding NW arrays were readily fabricated on the Si substrates after removing the AAO and  $\text{SiO}_2$  templates.

It is noteworthy that our hybrid process of  $\text{Si}_{1-x}\text{Ge}_x$  SEG and self-assembled nanotemplates offer the versatile controllability in aspect of not only dimension, position, growth direction of  $\text{Si}_{1-x}\text{Ge}_x$  nanostructures but also chemical composition. The dimension and position of the holes of nanotemplates, viz., AAO and DBC, can be deliberately controlled by altering the fabrication condition; varying the anodization condition for the AAO such as applied voltage, anodization time, and pore-widening time, and altering the molecular weight of each polymer block of DBC. Furthermore, the length scale of the  $\text{Si}_{1-x}\text{Ge}_x$  nanostructures can be readily controlled by changing the number of repeating cycles of  $\text{Si}_{1-x}\text{Ge}_x$  SEG. The chemical composition can be modulated by adjusting the flow rate of  $\text{Si}_2\text{H}_6$  and  $\text{GeH}_4$ . In addition, our approach presents the facile way to fabricate free-standing vertical  $\text{Si}_{1-x}\text{Ge}_x$  NW arrays on Si substrates without metal contamination. Finally, our hybrid fabrication process of  $\text{Si}_{1-x}\text{Ge}_x$  and self-assembled nanotemplates would shed light on the fabrication of well-controlled nanostructured building blocks for their reliable applications to future electronic applications.

#### Acknowledgment

This work was supported by the Technology Innovation Program funded by the Ministry of Knowledge Economy (MKE, Korea).

#### References

- [1] S. Kiravittaya, A. Rastelli, O.G. Schmidt, Rep. Prog. Phys. 72 (2009) 046502.
- [2] V. Schmidt, J.V. Wittemann, S. Senz, U. Gösele, Adv. Mater. 21 (2009) 2681.
- [3] M. Law, J. Goldberger, P.D. Yang, Annu. Rev. Mater. Res. 34 (2004) 83.
- [4] W. Lu, C.M. Lieber, J. Phys. D 39 (2006) R387.
- [5] P. Moriarty, Rep. Prog. Phys. 64 (2001) 297.
- [6] J. Stangl, V. Holy, G. Bauer, Rev. Mod. Phys. 76 (2004) 725.
- [7] S. Barth, F. Hernandez-Ramirez, J.D. Holmes, A. Romano-Rodriguez, Prog. Mater. Sci. 55 (2010) 563.
- [8] Y. Li, F. Qian, J. Xiang, C.M. Lieber, Mater. Today 9 (2006) 18.
- [9] B.K. Teo, X.H. Sun, Chem. Rev. 107 (2007) 1454.
- [10] K.L. Wang, D.H. Cha, J.L. Liu, C. Chen, Proc. IEEE 95 (2007) 1866.
- [11] I. Berbezier, A. Ronda, Surf. Sci. Rep. 64 (2009) 47.
- [12] D.J. Paul, Semicond. Sci. Technol. 19 (2004) R75.
- [13] U. Givan, F. Patolsky, Nano Lett. 9 (2009) 1775.
- [14] C. Qi, G. Goncher, R. Solanki, J. Jordan, Nanotechnology 18 (2007) 075302.
- [15] K.K. Lew, L. Pan, E.C. Dickey, J.M. Redwing, Adv. Mater. 15 (2003) 2073.
- [16] U. Givan, M. Kwait, F. Patolsky, J. Phys. Chem. C 114 (2010) 4331.
- [17] J.-M. Baribeau, X. Wu, N.L. Rowell, D.J. Lockwood, J. Phys. Condens. Matter 18 (2006) R139.
- [18] O. Pchelyakov, Y. Bolkhovityanov, A. Dvurechenskii, L. Sokolov, A. Nikiforov, A. Yakimov, B. Voigtländer, Semiconductors 34 (2000) 1229.
- [19] A. Rastelli, M. Stoffel, U. Denker, T. Merdzhanova, O.G. Schmidt, Phys. Status Solidi A 203 (2006) 3506.
- [20] J.E. Allen, E.R. Hemesath, D.E. Perea, J.L. Lensch-Falk, Z.Y. Li, F. Yin, M.H. Gass, P. Wang, A.L. Bleloch, R.E. Palmer, L.J. Lauhon, Nat. Nanotechnol. 3 (2008) 168.
- [21] J.B. Jackson, D. Kapoor, S.G. Jun, M.S. Miller, J. Appl. Phys. 102 (2007) 054310.
- [22] L. Vescan, T. Stoica, E. Sutter, Appl. Phys. A 87 (2007) 485.
- [23] L.H. Nguyen, V. Le Thanh, M. Halbwax, D. Débarre, V. Yam, F. Fossard, P. Boucaud, F. Meyer, D. Bouchier, Superlattices Microstruct. 36 (2004) 193.
- [24] Y.D. Wang, K.Y. Zang, S.J. Chua, J. Appl. Phys. 100 (2006) 054306.
- [25] O. Jessensky, F. Muller, U. Gösele, Appl. Phys. Lett. 72 (1998) 1173.
- [26] M. Li, C.K. Ober, Mater. Today 9 (2006) 30.
- [27] A.P. Li, F. Muller, A. Birner, K. Nielsch, U. Gösele, J. Appl. Phys. 84 (1998) 6023.
- [28] J.Y. Liang, H. Chik, A.J. Yin, J. Xu, J. Appl. Phys. 91 (2002) 2544.
- [29] I.W. Hamley, Nanotechnology 14 (2003) R39.
- [30] C. Park, J. Yoon, E.L. Thomas, Polymer 44 (2003) 6725.
- [31] D. Routkevitch, A.A. Tager, J. Haruyama, D. Almalawli, M. Moskovits, J.M. Xu, IEEE Trans. Electron Devices 43 (1996) 1646.
- [32] A.R. Choi, S.S. Choi, J.T. Kim, D.H. Cho, T.H. Han, K.H. Shim, Appl. Surf. Sci. 254 (2008) 6081.
- [33] M. Kolahdouz, J. Hallstedt, M. Ostling, R. Wise, H.H. Radamson, J. Electrochem. Soc. 156 (2009) H169.
- [34] L. Vescan, Mater. Sci. Eng. B 28 (1994) 1.
- [35] W.-H. Kim, S.-J. Park, J.-Y. Son, H. Kim, Nanotechnology 19 (2008) 045302.
- [36] S.-J. Kim, W.J. Maeng, S.K. Lee, D.H. Park, S.H. Bang, H. Kim, B.-H. Sohn, J. Vac. Sci. Technol., B 26 (2008) 189.
- [37] L. Vescan, C. Dieker, A. Hartmann, A. Vanderhart, Semicond. Sci. Technol. 9 (1994) 387.
- [38] T. Shimizu, T. Xie, J. Nishikawa, S. Shingubara, S. Senz, U. Gösele, Adv. Mater. 19 (2007) 917.
- [39] J.M. Hartmann, M. Burdin, G. Rolland, T. Billon, J. Cryst. Growth 294 (2006) 288.